Accelerating Convergence in Iterative Solution for Large-Scale Complete Active Space Self-Consistent-Field Calculations

DATASET *in* INTERNATIONAL JOURNAL OF QUANTUM CHEMISTRY · MARCH 2009

Impact Factor: 1.43

5 AUTHORS, INCLUDING:

Debashree Ghosh
CSIR - National Chemical Laboratory, Pune
20 PUBLICATIONS **60** CITATIONS

Accelerating Convergence in Iterative Solution for Large-Scale Complete Active Space Self-Consistent-Field Calculations

TAKESHI YANAI,[1] YUKI KURASHIGE,[1] DEBASHREE GHOSH,[2] GARNET KIN-LIC CHAN[2]

[1]*Department of Theoretical and Computational Molecular Science, Institute for Molecular Science, Okazaki, Aichi 444-8585, Japan*

[2]*Department of Chemistry and Chemical Biology, Cornell University, Ithaca, NY 14853-1301*

Received 2 November 2008; accepted 6 January 2009
Published online 23 March 2009 in Wiley InterScience (www.interscience.wiley.com).
DOI 10.1002/qua.22099

ABSTRACT: An algorithm that accelerates the convergence of the iterative optimization of the complete active space self-consistent field (CASSCF) wavefunction so as to find a optimum solution in fewer macroiterations is described. The algorithm is oriented to large-scale CASSCF problems that are to be solved with a combination of density matrix renormalization group (DMRG) method for the configuration interaction (CI) process. The algorithm is based on the alternating (or two-step) CASSCF optimization in which the CI and molecular orbital (MO) parameters are optimized

Correspondence to: T. Yanai; e-mail: yanait@ims.ac.jp

Contract grant sponsors: Cornell University, Cornell Center for Materials Research (CCMR), David and Lucile Packard Foundation, Alfred P. Sloan Foundation, Core Research for Evolutional Science and Technology Program, Japan Science and Technology Agency (JST), Research Center for Computational Science, Okazaki Japan.

Contract grant sponsor: National Science Foundation CAREER Program.

Contract grant number: CHE-0645380.

Contract grant sponsor: Department of Energy, Office of Science.

Contract grant number: DE-FG02-07ER46432.

Contract grant sponsor: Ministry of Education, Culture, Sports, Science and Technology, Japan (MEXT) (Priority Areas for "Molecular Theory for Real Systems").

Contract grant number: 461.

separately. Convergence ratio is improved by finding further optimized MOs from a linear extrapolation of the MO sets of the iteration history. The acceleration results in fewer diagonalizations in a total CASSCF calculation to save a considerable computational cost. The convergence performance is examined in a couple of realistic applications on SiC_3 and poly(phenyl)carbenes. For poly(phenyl)carbenes, the large-size CASSCF calculations with CAS(30e,30o) that entails full π valence space as well as sp^2 orbital space of carbenes are performed by using the practical implementation of DMRG-CASSCF in conjunction with the acceleration technique. © 2009 Wiley Periodicals, Inc. Int J Quantum Chem 109: 2178–2190, 2009

Key words: DMRG-CASSCF; multireference; strong correlation; carbine; orbital optimization

1. Introduction

Posing the multireference problems in quantum chemistry, the complex electronic structures troubling the problems ought to be described by handling multiple electronic configurations, several of which should be equally important in the description. One of the well-established prescriptions to construct the multiconfigurational electronic wavefunctions is the complete active space self-consistent field (CASSCF) method, which is one kind of multiconfigurational self-consistent field (MCSCF) theory [1–14]. The CASSCF method is usefully applied to chemical theory problems such as exploring chemical reactions of bonding, dissociation, and isomerization along the reaction coordinates, electronically excited states, unstable electronic structures of radical systems, and multiple covalent bindings in molecular metal complexes, etc.

Defining the structure of the CASSCF wavefunction is somewhat manual and thus requires us to (semi-)manually select a finite size of the active orbital space, which is usually made by valence electrons and orbitals of chemical importance, so as to cover as many relevant electronic configurations as possible by using the concomitant Slater determinants. The CASSCF model describes the static electron correlation by fully correlating the active electrons within the active orbitals from the full configuration interaction (CI) diagonalization of the active space Hamiltonian. Concurrently, the CASSCF method carries out the iterative search for the optimal molecular orbital (MO) basis, which are regarded as the mean-field representations of the statically correlated many-electron wavefunction.

The CASSCF wavefunction is often used for the subsequent multireference calculations that further compute the dynamic correlation for the purpose of attaining the quantitative chemical accuracy on top of the prior CASSCF multireference setting which delivers a reasonable qualitative accuracy beforehand. The second-order perturbation methodology from the CAS reference, such as the multireference Møller-Plesset theory (MRMP) of Hirao [15–20], the multiconfigurational quasi-degenerate perturbation theory (MCQDPT) of Nakano [21–24], the complete active space perturbation theory (CASPT2) of Roos and coworkers [25, 26], and other similar approaches, has been successfully practiced in a lot of large multireference electronic structure problems in a computationally efficient manner.

We have recently presented an extensively large-scale CASSCF approach, which is realized by implementing the orbital optimization with the density matrix renormalization group (DMRG) wavefunction (DMRG-CASSCF) [27]. Another implementation of the orbital-optimized DMRG has been reported by Zgid and Nooijen around the same time [28, 29]. By virtue of the compact nature of the DMRG wavefunction [27–49], which provides an efficient description of the strongly correlated electronic structures, the DMRG-CASSCF approach [27–29] enables us to handle much larger active spaces than are possible with the traditional CASSCF algorithm. Using the DMRG-CASSCF method, we calculated the low-lying excited states in π-conjugated polyenes up to $C_{24}H_{26}$ by correlating complete π-valence space (corresponding to CAS(24e,24o) for the largest), while the previous best calculations on these system by Hirao group [50–52] had to use incomplete π-valence space in the CASSCF calculations which were limited to CAS(10e,10o) (five nominal double bonds) even for the $C_{24}H_{26}$ system.

The computational determination of the CASSCF wavefunction represents a nonlinear mathematical problem. The iterative solution is thus necessitated to search for an optimum form of the wavefunction

in the determinant space as well as the optimum MOs. The way of optimizing the CASSCF wavefunction has been well established nowadays. Exploiting the second-order form of the energy function and the exponential parameterization for the orbital space, the affordable CASSCF optimizations have been routinely carried out. This article describes how to efficiently accelerate the iterative optimization of CASSCF wavefunction in terms of further reducing the number of iterations that reach to the convergence. In particular, our purpose is to make the algorithm tailored to the computational demand to realize fewer exact diagonalizations with DMRG during the DMRG-CASSCF calculation. In the next section, we describe the details of the accelerated optimization that is fitted to the purpose. In Section 3 we present the computational performances of the algorithm from its implementation. Conclusions are given in Section 4.

2. Algorithm

2.1. THE SECOND-ORDER CASSCF OPTIMIZATION

The finding of solution in the CASSCF method is to iteratively minimize the energy with respect to the multiconfigurational wavefunction in a self-consistent fashion. Many of the well-established CASSCF implementations [7, 9, 13] find the minimum by using the second-order optimization based on the Newton–Raphson (NR) algorithm in which to search a root of the energy gradient with respect to both CI and MO coefficients, which are an entire set of the variational parameters of the wavefunction. The NR optimization delivers the quadratic (second-order) convergence to some neighborhood of a solution.

On the large-scale CAS settings, supposing very complicated multireference problems that require an immense size of CI space (e.g., 1 peta ($= 10^{12}$) dimensions) for the multireference representations, the computational expense of dealing with such a number of CI parameters in the NR procedure is formidable. It is even more impractical to compute and store the derivatives of the energy with respect to the CI coefficients, the number of which grows in a factorial scale with the problem size. While the DMRG method [27–49] provides a compact entangled form of the large multiconfiguration wavefunction, the computational treatment of the energy gradient with respect to the DMRG parameterization of the wavefunction is not so easy or simple to combine with the second-order update to the wavefunction. (It should be mentioned, however, that computing the energy gradient with respect to the DMRG wavefunction parameters is not impossible according to the response theory and may be efficient as well.)

Our implementation has thus simply adopted the alternating (or two-step) optimization, which is widely used, where the CI and MO parameters are optimized separately. The separated optimizations are alternated during the so-called macroiterations, in which the MOs are optimized by the second-order minimization with the CI coefficients fixed while the Hamiltonian in the optimized MO basis is diagonalized to update the CI representation. The two-step algorithm can avoid the differentiations of the energy with respect to the CI parameters, whereas it may lose the maximum convergence speed from the full second-order minimization (i.e. one-step algorithm). In the two-step algorithm, the CI diagonalization, which is an expensive step in every macroiteration, is iterated many times until the convergence. Thus, this study focuses central attention on how to improve the convergence behavior of the alternating iterations to realize fewer diagonalizations for saving the total cost.

Here we begin with a brief review on the second-order optimization for the MOs in the two-step CASSCF method. From the guess, a set of the initial MOs $\{\phi_p^{(0)}(r)\}$ is given by

$$\phi_p^{(0)}(r) = \sum_\mu \chi_\mu(r) C_{\mu p}^{(0)}, \tag{1}$$

which are the linear combinations of the atomic orbitals (AOs) $\{\chi_\mu(r)\}$, where $\mathbf{C}^{(0)}$ is the coefficient matrix of the guess MOs. In the given MO basis $\{\phi_p^{(0)}(r)\}$, a spin-free form of the electronic Hamiltonian is constructed as

$$\hat{H}^{(0)} = \sum_{pq} h_{pq} \hat{E}_{pq} + \frac{1}{2} \sum_{pqrs} (pq|rs)(\hat{E}_{pq}\hat{E}_{rs} - \delta_{qr}\hat{E}_{ps}), \tag{2}$$

where the one- and two-electron integrals h_{pq} and $(pq|rs)$ are calculated from the AO integrals as follows:

$$h_{pq} = \sum_{\mu\nu} \langle \chi_\mu | \hat{h} | \chi_\nu \rangle C_{\mu p}^{(0)} C_{\nu q}^{(0)}, \tag{3}$$

$$(pq|rs) = \sum_{\mu\nu}(\chi_\mu\chi_\nu|\chi_\rho\chi_\sigma)C^{(0)}_{\mu p}C^{(0)}_{\nu q}C^{(0)}_{pr}C^{(0)}_{\sigma s}, \quad (4)$$

and the generator is defined by $\hat{E}_{pq} = a^\dagger_{p\alpha}a_{q\alpha} + a^\dagger_{p\beta}a_{q\beta}$.

The CAS reference is set up by partitioning the MOs into three sets of the closed-shell, active, and virtual orbitals. According to the orbital partitioning, the active space Hamiltonian $\hat{H}^{(0)}_{\rm act}$ is given by

$$\hat{H}^{(0)}_{\rm act} = E^{\rm closed} + \sum_{ij}h^{\rm act}_{ij}\hat{E}_{ij} + \frac{1}{2}\sum_{ijkl}(ij|kl)(\hat{E}_{ij}\hat{E}_{kl} - \delta_{jk}\hat{E}_{il}), \quad (5)$$

where the indexes i, j, k, l are limited to the active orbitals and the modified one-electron integrals and closed-shell energy are given respectively by

$$E^{\rm closed} = 2\sum_c h_{cc} + \sum_{cc'}\{2(cc|c'c') - (cc'|c'c)\}, \quad (6)$$

$$h^{\rm act}_{ij} = h_{ij} + \sum_c\{2(ij|cc) - (ic|cj)\}, \quad (7)$$

where c, c' denote the closed-shell indexes. The CAS wavefunction $|\Psi^{(0)}\rangle$, which describes a full correlation of the active electrons within the active orbitals, is obtained as an eigenstate of the active space Hamiltonian $H^{(0)}_{\rm act}$ via the exact diagonalization,

$$\hat{H}^{(0)}_{\rm act}|\Psi^{(0)}\rangle = E^{(0)}_{\rm CAS}|\Psi^{(0)}\rangle. \quad (8)$$

The energy $E^{(0)}_{\rm CAS}$ is an expectation value of not only $\hat{H}^{(0)}_{\rm act}$ but also $\hat{H}^{(0)}$,

$$E^{(0)}_{\rm CAS} = \langle\Psi^{(0)}|\hat{H}^{(0)}_{\rm act}|\Psi^{(0)}\rangle = \langle\Psi^{(0)}|\hat{H}^{(0)}|\Psi^{(0)}\rangle. \quad (9)$$

From $|\Psi^{(0)}\rangle$, we compute the one- and two-electron reduced density matrix (RDM) elements of the active space $\gamma^{(0)}_{ij}$ and $\gamma^{(0)}_{ij,kl}$,

$$\gamma^{(0)}_{ij} = \langle\Psi^{(0)}|\hat{E}_{ij}|\Psi^{(0)}\rangle, \quad (10)$$

$$\gamma^{(0)}_{ij,kl} = \langle\Psi^{(0)}|\hat{E}_{ij}\hat{E}_{kl} - \delta_{jk}\hat{E}_{il}|\Psi^{(0)}\rangle, \quad (11)$$

and the energy expectation value can be rewritten with the RDMs as

$$E^{(0)}_{\rm CAS} = E^{\rm closed} + \sum_{ij}h^{\rm act}_{ij}\gamma^{(0)}_{ij} + \frac{1}{2}\sum_{ijkl}(ij|kl)\gamma^{(0)}_{ij,kl}. \quad (12)$$

The orbital optimization is carried out with a unitary transformation that rotates the MOs as

$$\psi^{(1)}_{p'}(r) = \sum_p \Psi^{(0)}_p(r)U^{(0)}_{pp'}, \quad (13)$$

which is represented as rotating the MO coefficient matrix,

$$\mathbf{C^{(1)} = C^{(0)}U^{(0)}}. \quad (14)$$

For the unitary matrix $\mathbf{U}^{(0)}$, the following exponential parameterization is widely used,

$$\mathbf{U}^{(0)} = \exp(\mathbf{X}^{(0)}) \quad (15)$$

where $\mathbf{X}^{(0)}$ is the alternative parameter matrix to be optimized and is antisymmetric, $\mathbf{X}^{(0)\dagger} = -\mathbf{X}^{(0)}$. With the CI structure of the wavefunction $|\Psi^{(0)}\rangle$ fixed, the energy function of the orbital rotation, $E^{(0)}(\mathbf{X}^{(0)})$, is given by

$$E^{(0)}(\mathbf{X}^{(0)}) = \langle\Psi^{(0)}|e^{-\hat{X}^{(0)}}\hat{H}^{(0)}e^{\hat{X}^{(0)}}|\Psi^{(0)}\rangle, \quad (16)$$

where

$$\hat{X}^{(0)} = \sum_{pq}X^{(0)}_{pq}\hat{E}_{pq}. \quad (17)$$

The NR algorithm exploit an approximation of the energy function $E^{(0)}(\mathbf{X}^{(0)})$ [Eq. (16)] into the quadratic function,

$$E^{(0)}(\mathbf{X}^{(0)}) \approx E^{(0)}_{\rm CAS} + \mathbf{g}^{(0)\dagger}\mathbf{X}^{(0)} + \frac{1}{2}\mathbf{X}^{(0)\dagger}\mathbf{H}^{(0)}\mathbf{X}^{(0)}, \quad (18)$$

upon which the stationary point locating the approximate minimum is employed as the optimal rotation step for $\mathbf{X}^{(0)}$. To that end, we solve the following stationary equation to obtain the rotation step,

$$\mathbf{H}^{(0)}\mathbf{X}^{(0)} = -\mathbf{g}^{(0)}, \quad (19)$$

where $\mathbf{g}^{(0)}$ and $\mathbf{H}^{(0)}$ are the gradient vector and Hessian matrix of the energy function, respectively, which are expressed as follows:

$$g^{(0)}_{pq} = \frac{\partial E^{(0)}}{\partial X_{pq}} = \langle \Psi^{(0)} | [\hat{H}^{(0)}, \hat{E}^{-}_{pq}] | \Psi^{(0)} \rangle, \quad (20)$$

$$H^{(0)}_{pq,rs} = \frac{\partial E^{(0)}}{\partial X_{pq} \partial X_{rs}} = \frac{1}{2} \{ \langle \Psi^{(0)} | [[\hat{H}^{(0)}, \hat{E}^{-}_{pq}], \hat{E}^{-}_{rs}] | \Psi^{(0)} \rangle + \langle \Psi^{(0)} | [[\hat{H}^{(0)}, \hat{E}^{-}_{rs}], \hat{E}^{-}_{pq}] | \Psi^{(0)} \rangle \}, \quad (21)$$

where $\hat{E}^{-}_{pq} = \hat{E}_{pq} - \hat{E}_{qp}$. The one- and two-electron RDMs, $\gamma^{(0)}_{ij}$ and $\gamma^{(0)}_{ij,kl}$, are used for the evaluation of the above derivative elements. If the gradients vector $\mathbf{g}^{(0)}$ is zero, the energy is already minimized. Lengsfield suggested to use the lowest root of the following eigen-equation with the augmented Hessian [3, 4],

$$\begin{pmatrix} 0 & \mathrm{g}^{(0)\dagger} \\ \mathbf{g}^{(0)} & \mathbf{H}^{(0)}/\lambda \end{pmatrix} \begin{pmatrix} 1/\lambda \\ \mathbf{X}^{(0)} \end{pmatrix} = \epsilon \begin{pmatrix} 1/\lambda \\ \mathbf{X}^{(0)} \end{pmatrix} \quad (22)$$

subject to $\epsilon = \lambda \mathrm{g}^{(0)\dagger} \mathbf{X}^{(0)}$, instead of using the solution of the linear equation of Eq. (19), for the better-conditioned rotation that significantly improves the convergence. Our implementation solves Eq. (22) of the stationary condition by the iterative subspace method, whose computation cost is usually moderate.

We briefly summarize the iterative procedure of the two-step CASSCF optimization, as follows:

0. Initialize $\mathrm{C}^{(0)}$ for the MOs $\{\phi^{(0)}_p(r)\}$, and $I \leftarrow 0$.

1. Set up the Hamiltonian $\hat{H}^{(I)}$ in $\{\phi^{(I)}_p(r)\}$ [Eq. (2)], by which the CAS wavefunction $|\Psi^{(I)}\rangle$ is determined from Eq. (8). Evaluate one- and two-electron RDMs $\gamma^{(I)}_{ij}$ and $\gamma^{(I)}_{ij,kl}$ of $|\Psi^{(I)}\rangle$.

2. Find the orbital rotation step $\mathbf{X}^{(I)}$ from the stationary condition, and the new orbitals are obtained as

$$\mathbf{C}^{(I+1)} = \mathbf{C}^{(I)} \exp(\mathbf{X}^{(I)}), \quad (23)$$

and $I \leftarrow I + 1$.

Steps 1 and 2, which constitute a single macroiteration, are iterated until the gradient $\mathbf{g}^{(I)}$ is small enough.

2.2. ACCELERATION ALGORITHM REDUCING THE TOTAL NUMBER OF THE MACROITERATIONS

We now describe an algorithm that speeds up the convergence of the minimum search in the CASSCF optimization so as to find the minimum in fewer macroiterations whereby the total number of diagonalizations carried out can be reduced. From the outline of the two-step CASSCF procedure that we just reviewed previously, it can been seen that by giving a set of MOs ($\mathbf{C}^{(I)}$) as an input, the energy gradient $\mathbf{g}^{(I)}$ is obtained as its output, just as a map f:$\mathbf{C}^{(I)} \rightarrow \mathbf{g}^{(I)}$ through the following association:

$$\mathbf{C}^{(I)} \rightarrow \hat{H}^{(I)} \rightarrow \{|\Psi^{(I)}\rangle, \gamma^{(I)}\} \rightarrow \mathbf{g}^{(I)}. \quad (24)$$

The goal of the CASSCF optimization is therefore viewed as locating the MO coefficients $\mathrm{C}^{(I)}$ such that the corresponding gradient $\mathbf{g}^{(I)}$ is zero. We here propose a way of achieving the goal by further optimizing the MO set from a linear extrapolation of the MO sets of the iteration history. The extrapolation scheme is based on the direct inversion of iterative subspace (DIIS) method [53], by which the norm of the gradient associated with the extrapolated MO set is to be minimized. Note that Zgid and Nooijen also noted the similar extrapolation scheme in their most recent article on the orbital-optimized DMRG implementation while they observed it by analogy with the DIIS acceleration for the coupled-cluster calculations [29]. Hamilton and Pulay also applied the DIIS method to simple multiconfigurational SCF wavefunctions to speed up the convergence of the first-order Fock matrix-based technique, which though corresponds to the one-step optimization algorithm [54].

For that purpose, the following exponential representation is again introduced,

$$\mathbf{C}^{(I)} = \mathbf{C}^{(0)} U^{(I)}, \quad (25)$$

$$U^{(I)} = \exp(\mathbf{A}^{(I)}), \quad (26)$$

where the unitary matrix $U^{(I)}$ describes a rotation from the initial orbitals to the ones updated from the NR stationary condition of the orbital optimization, and is thus given according to Eqs. (14), (15), and (23) by the following consecutive matrix multiplications,

$$U^{(I)} = \mathbf{U}^{(0)} \mathbf{U}^{(1)} \cdots \mathbf{U}^{(I-1)} = e^{\mathbf{X}^{(0)}} e^{\mathbf{X}^{(1)}} \cdots e^{\mathbf{X}^{(I-1)}}, \quad (27)$$

and $U^{(0)}$ given by the identity matrix. Note that the exponent matrix $\mathrm{A}^{(I)}$ can be calculated from the relation $\mathbf{A}^{(I)} = \log(U^{(I)})$. Our algorithm improves the MO set by the following linear extrapolation of the rotation matrices of the past macroiterations,

$$\tilde{\mathbf{A}}^{(I)} = \sum_{\mu=1,\ldots,I} c_\mu \mathbf{A}^{(\mu)}, \tag{28}$$

where c_μ are extrapolation coefficients that are determined from a linear subspace solver of the DIIS algorithm in which the gradients of each macroiteration are used as the DIIS error vectors. Noticing that the MO basis of representing the gradient elements $g_{pq}^{(I)}$ varies during the macroiterations, we represent the gradient elements in the AO basis, which is consistent over the macroiterations, for the DIIS error vectors,

$$\mathrm{g}_{\mathrm{AO}}^{(I)} = (\mathbf{C}^{(I)})^{-1\dagger} \mathrm{g}^{(I)} (\mathbf{C}^{(I)})^{-1}, \tag{29}$$

where $(\mathbf{C}^{(I)})^{-1} = \mathbf{C}^{(I)\dagger}\mathbf{S}^{\mathrm{AO}}$ and $S_{\mu\nu}^{\mathrm{AO}} = \langle \chi_\mu | \chi_\nu \rangle$, so that the matrix elements of the DIIS least square fitting are given as

$$B_{IJ} = \mathrm{g}_{\mathrm{AO}}^{(I)\dagger} \mathrm{g}_{\mathrm{AO}}^{(J)}. \tag{30}$$

The coefficient matrix of the refined MOs is eventually obtained from the extrapolated rotation matrix $\tilde{\mathrm{A}}^{(I)}$ as

$$\tilde{\mathbf{C}}^{(I)} = \mathbf{C}^{(0)} \exp(\tilde{A}^{(I)}). \tag{31}$$

In the practical implementation, the DIIS acceleration should only be turned on if the MOs are sufficiently stable, reaching near convergence.

2.3. STATIONARY CONDITION SOLVER IN NATURAL ORBITAL BASIS

In each orbital optimization step, we solve iteratively a large system of linear equations given by Eqs. (19) and (22). The linear equation is represented in the basis of the orbital rotation space, that is the first-order one-particle interacting space, as described in Eq. (17), namely the singly-external excitations of closed-shell↔ active, closed-shell↔ virtual, and active↔ virtual orbitals,

$$(\hat{E}_{ci} - \hat{E}_{ic}) |\Psi^{(I)}\rangle, \tag{32}$$

$$(\hat{E}_{ca} - \hat{E}_{ac}) |\Psi^{(I)}\rangle, \tag{33}$$

$$(\hat{E}_{ia} - \hat{E}_{ai}) |\Psi^{(I)}\rangle, \tag{34}$$

respectively, where c, i, and a denote indexes of the closed-shell, active, virtual orbitals, respectively. Note that the space size is thus $n_{\mathrm{c}}n_{\mathrm{a}} + n_{\mathrm{c}}n_{\mathrm{v}} + n_{\mathrm{a}}n_{\mathrm{v}}$ where n_{c}, n_{a}, and n_{v} are the numbers of the closed-shell, active, and virtual orbitals, respectively. This interacting space is, in general, nonorthogonal and often nearly linearly dependent, resulting in poor convergence rate in the iterative solution.

To make the equation better-conditioned, the first-order interacting basis is orthogonalized by diagonalizing its overlap,

$$S_{pq,p'q'} = \langle \Psi^{(I)} | (\hat{E}_{pq} - \hat{E}_{qp})^\dagger (\hat{E}_{p'q'} - \hat{E}_{q'p'}) | \Psi^{(I)} \rangle. \tag{35}$$

Specifically, the overlap matrix is expressed as follows:

$$S_{ci,c'i'} = \delta_{cc'}(\delta_{ii'} - \gamma_{ii'}^{(I)}), \tag{36}$$

$$S_{ca,c'a'} = 2\delta_{cc'}\delta_{aa'}, \tag{37}$$

$$S_{ia,i'a'} = \delta_{aa'}\gamma_{ii'}^{(I)}, \tag{38}$$

where δ_{ij} is Kronecker delta. According to these, the choice of natural orbitals (NOs) for the active orbital basis makes the overlap matrices naturally diagonal since the one-electron RDM in NO basis is a diagonal matrix.

Hence, we transform the MO coefficient matrix $\mathbf{C}^{(I)}$ into the NO representation every macroiteration when entering the orbital optimization step,

$$\mathbf{C}_{\mathrm{NO}}^{(I)} = \mathbf{C}^{(I)} \mathbf{U}_{\mathrm{NO}}^{(I)}, \tag{39}$$

where $\mathbf{U}_{\mathrm{NO}}^{(I)}$ is a unitary matrix that consists of the eigenvectors of the one-electron RDM $\gamma_{ii'}^{(I)}$, namely,

$$\mathbf{U}_{\mathrm{NO}}^{(I)\dagger} \gamma_{ii'}^{(I)} \mathbf{U}_{\mathrm{NO}}^{(I)} = \mathbf{n}_{\mathrm{occ}}, \tag{40}$$

and the eigenvalues $\mathbf{n}_{\mathrm{occ}}$ correspond to the occupation numbers. In the NO basis, the rotation step $\mathbf{X}^{(I)}$ is determined as a solution of the stationary equation, which is better-conditioned in this basis. An extra treatment is taken to transform back the optimized MOs by $\mathbf{U}_{\mathrm{NO}}^{(I)}$, for the purpose of a consistent combination with the DIIS acceleration. Therefore, the coefficient matrix of the MOs that are optimized from the NR stationary condition is finally expressed as

$$\mathbf{C}^{(I+1)} = \mathbf{C}^{(I)} \{ \mathbf{U}_{\mathrm{NO}}^{(I)} \exp(\mathbf{X}^{(I)}) \mathbf{U}_{\mathrm{NO}}^{(I)\dagger} \} \tag{41}$$

which is a counterpart of Eq. (23).

2.4. THE ACCELERATED TWO-STEP DMRG-CASSCF METHOD

The acceleration algorithms presented in this study can be easily combined with the orbital-optimized DMRG (i.e., DMRG-CASSCF) implementation. What we should additionally pay attention to when the DMRG is used for the CI step is an extra orbital rotation to localize the active space orbitals before every DMRG calculation, as described in a previous article [27]. The following is the detailed complete procedure of the accelerated DMRG-CASSCF optimization at the I-th macroiteration ($I = 0, 1, \ldots$).

1. Localize the active space orbitals (LO),

$$\mathbf{C}_{\mathrm{LO}}^{(I)} \leftarrow \mathbf{C}^{(I)}\mathbf{U}_{\mathrm{LO}}^{(I)}. \tag{42}$$

2. Build the active space Hamiltonian $\hat{H}_{\mathrm{act}}^{(I)}$ [Eq. (5)] in the LO basis.
3. Perform the DMRG diagonalization of $\hat{H}_{\mathrm{act}}^{(I)}$ and assemble the one- and two-electron RDMs $\gamma_{ij}^{(I)\mathrm{LO}}$ and $\gamma_{ij,kl}^{(I)\mathrm{LO}}$ [27, 28].
4. Transform back the basis from the localized representation against the orbitals and RDM elements,

$$\mathbf{C}^{(I)} \leftarrow \mathbf{C}_{\mathrm{LO}}^{(I)}\mathbf{U}_{\mathrm{LO}}^{(I)\dagger},$$
$$\gamma_{ij}^{(I)} \leftarrow \gamma_{ij}^{(I)\mathrm{LO}} \quad \text{and} \quad \gamma_{ij,kl}^{(I)} \leftarrow \gamma_{ij,kl}^{(I)\mathrm{LO}} \tag{43}$$

5. Diagonalize the one-electron RDM $\gamma_{ij}^{(I)}$, to obtain the natural orbitals,

$$\mathbf{C}_{\mathrm{NO}}^{(I)} \leftarrow \mathbf{C}^{(I)}\mathbf{U}_{\mathrm{NO}}^{(I)}, \tag{44}$$

and transform the one- and two-electron RDMs into the NO basis, $\gamma_{ij}^{(I)\mathrm{NO}} \leftarrow \gamma_{ij}^{(I)}$ and $\gamma_{ij,kl}^{(I)\mathrm{NO}} \leftarrow \gamma_{ij,kl}^{(I)}$

6. Build the full orbital space Hamiltonian $\hat{H}^{(I)}$ [Eq. (2)] in the NO basis.
7. Solve the linear equation of the orbital stationary condition with the augmented Hessian matrix, in which the gradient vector $\mathbf{g}^{(I)}$ and Hessian matrix $\mathbf{H}^{(I)}$ are constructed in the NO basis representation. As the solution, the rotation step $\mathbf{X}^{(I)}$ is obtained.
8. Calculate the total rotation exponent matrix $\mathbf{A}^{(I+1)} = \log(U^{(I+1)})$ where

$$U^{(I+1)} = U^{(I)}\{\mathbf{U}_{\mathrm{NO}}^{(I)}\exp(\mathrm{X}^{(I)})\mathbf{U}_{\mathrm{NO}}^{(I)\dagger}\}, \tag{45}$$

which is the equivalence of Eq. (41).

9. Transform the gradient vector into the AO basis representation, $\mathrm{g}^{(I)} \rightarrow \mathrm{g}_{\mathrm{AO}}^{(I)}$ and obtain the DIIS extrapolation coefficients by forming the least square fitting matrix [Eq. (30)] from the gradient vectors of the past macroiterations.
10. Calculate the refined MOs $\tilde{\mathbf{C}}^{(I+1)}$ from the extrapolation by Eqs. (28) and (31).
11. $\mathbf{C}^{(I+1)} \leftarrow \tilde{\mathbf{C}}^{(I+1)}$.

In the DMRG-CASSCF, the accuracy of our active space DMRG wavefunction depends on the user-specified size of renormalized basis to be retained (M), but in this study we will use sufficiently large M so that our wavefunction is nearly an exact eigenfunction of the active space Hamiltonian, and we can omit active-active rotations.

3. Results

3.1. CONVERGENCE OF CASSCF ITERATIONS WITH SiC_3 OF $^1A_1$ AND $^3B_2$ STATES

The convergence performance of the CASSCF energy minimizations was examined with the moderate-size benchmark problems, for which we calculated the electronic structures of SiC_3. The stable structure of SiC_3 has been investigated by using several theoretical approaches such as the CISD + Q [55], CCSD(T) [56], MCQDPT with CASSCF [57], and GMC-PT [58] and MRMP-F12 [59] methods. High-level calculations by the CCSD(T) [56] and GMC-PT [58] methods predicted a rhomboidal isomer labeled as 2s, which is the $\mathbf{C}_{2v}$ point-group symmetry, to be the most stable.

For the geometrical parameters of SiC_3 in our model calculations, we used a structure of the 2s isomer that was optimized in Ref. [57] with 6-31G(d) basis set by the fully optimized reaction space (FORS) SCF method [8], which is equivalent to the CASSCF method. For the benchmark calculations, cc-pVQZ basis set [60, 61] was used and the MOs to be optimized were then represented with 224 AO basis functions. The initial MOs for the subsequent CASSCF calculations were taken from the canonical orbitals that were obtained by the restricted Hartree–Fock (RHF) calculation for the $^1A_1$ state, in which the HF energy is -402.35204366 E_h and the HF electronic configuration is made by

TABLE I

Total energies (in hartree) and norms of the gradient vectors (in a.u.) along macroiterations of CASSCF(10e, 10o) optimization for the $^1A_1$ state of SiC_3 with cc-pVQZ basis set.

One-step method			Two-step method					
						With DIIS accel.		
Iter.	Energy	Grad.	Iter.	Energy	Grad.	Iter.	Energy	Grad.
1	−402.37133979	2.8E-02	1	−402.37133978	2.8E-02			
2	−402.40103770	3.0E-02						
3	−402.41929290	1.6E-02	8	−402.46118588	1.2E-02			
4	−402.43407200	2.0E-02	9	−402.46297142	6.1E-03		DIIS turned on	
5	−402.45405242	2.6E-02	10	−402.46322367	2.4E-03	10	−402.46322367	2.4E-03
6	−402.46295956	1.4E-02	11	−402.46325580	8.1E-04	11	−402.46326059	2.2E-04
7	−402.46326053	5.9E-04	12	−402.46326027	2.8E-04	12	−402.46326101	5.3E-05
8	−402.46326107	4.1E-06	13	−402.46326095	1.0E-04	13	−402.46326107	9.7E-06
			14	−402.46326105	3.8E-05	14	−402.46326107	1.6E-06
			15	−402.46326107	1.5E-05			
			16	−402.46326107	5.8E-06			
			17	−402.46326107	2.3E-06			

16 doubly occupied orbitals and is expressed as $(\text{core})(6a_1)^2(7a_1)^2(3b_1)^2(8a_1)^2(2b_2)^2(4b_1)^2(9a_1)^2(10a_1)^2$.

We used CAS(10e,10o) for the reference space where 10 active electrons were fully correlated within 10 active orbitals, which were the 8-12a_1, 4-5b_1 and 2-4b_2 orbitals. The number of the closed-shell, active, virtual orbitals is thus (n_c, n_a, n_v)= (11, 10, 203). With this orbital partitioning, two target states $^1A_1$ and $^3B_2$ were specified for the state-specific CASSCF optimization of the wavefunctions and MO representations that were initialized with the RHF orbitals.

Tables I and II present the total energies and norms of the gradient vectors over the macroiterations of the CASSCF calculations. Figures 1 and 2 visualize the convergence progress by plotting the norms of the gradient vectors. For comparison, the tables and figures include the performance of the

TABLE II

Total energies (in hartree) and norms of the gradient vectors (in a.u.) along macroiterations of CASSCF(10e,10o) optimization for the $^3B_2$ state of SiC_3 with cc-pVQZ basis set.

One-step method			Two-step method					
						With DIIS accel.		
Iter.	Energy	Grad.	Iter.	Energy	Grad.	Iter.	Energy	Grad.
1	−402.27679658	2.0E-01	1	−402.27679674	2.0E-01			
2	−402.33145164	6.5E-02						
3	−402.35173716	2.5E-02	13	−402.38915392	1.4E-02			
4	−402.35978328	9.8E-03	14	−402.39064974	7.2E-03		DIIS turned on	
5	−402.36551682	7.5E-03	15	−402.39103630	3.4E-03	15	−402.39103630	3.4E-03
6	−402.37533012	2.1E-02	16	−402.39117409	1.9E-03	16	−402.39122432	1.5E-03
7	−402.38579400	2.9E-02	17	−402.39122551	1.2E-03	17	−402.39125198	4.3E-04
8	−402.39061532	1.7E-02	18	−402.39124443	7.6E-04	18	−402.39125497	1.9E-04
9	−402.39125366	8.4E-04	19	−402.39125140	4.9E-04	19	−402.39125565	5.6E-05
10	−402.39125571	2.4E-05	20	−402.39125402	3.2E-04	20	−402.39125571	1.5E-05
11	−402.39125571	6.0E-07	21	−402.39125503	2.1E-04	21	−402.39125571	2.1E-06
			22	−402.39125543	1.3E-04			
			32	−402.39125571	1.8E-06			

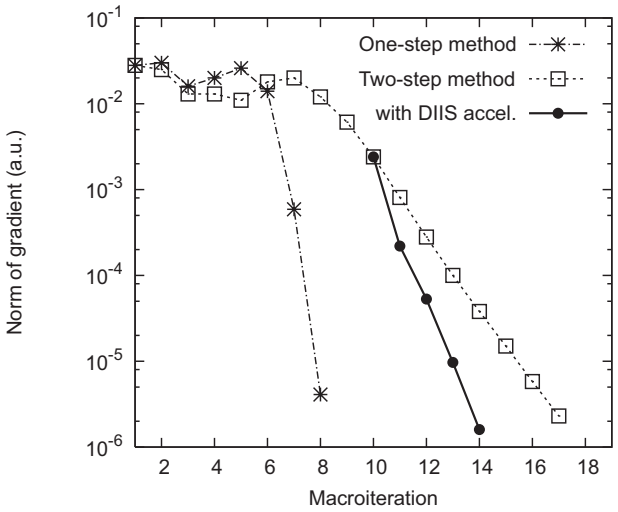

FIGURE 1. Convergence progress of norms of the gradient vectors in CASSCF(10e,10o) calculations for the $^1A_1$ state of SiC_3 with cc-pVQZ basis set.

one-step optimization with the augmented Hessian method, which was done with the different implementation on MOLPRO program package [62]. Note that the convergence behaviors observed from our implementation of the two-step optimization with the augmented Hessian method was reproduced by another similar implementation in MOLPRO for the same two-step method.

Turning on the DIIS acceleration at the 10-th and 15-th macroiteration for the $^1A_1$ and $^3B_2$ calculations, respectively, the two-step optimization quickly converged in 5 and 7 macroiterations for the respective states. As a result, the total number of the two-step macroiterations required to meet the convergence criteria was slightly moderated from 17 to 14 for the $^1A_1$ state and significantly reduced from 32 to 21 for the $^3B_2$ state. The $^3B_2$ state calculation was poorly converged without the DIIS acceleration. The initial RHF orbitals seem to be far from good guess for this state.

As described earlier, the one-step optimization converged at the maximum convergence rate. We should say, however, that it is not applicable to gigantic CAS calculations that are too large to handle the derivatives with respect to the CI parameters, as in the cases presented afterward with a combination of the DMRG method.

We have found that the DIIS combination accelerates the convergence of the two-step method by a few or dozens of macroiterations. Saving a few macroiterations is rather beneficial when the computational cost of the single CI calculation is demanding.

3.2. ENERGY DIFFERENCES BETWEEN SINGLET AND HIGH-SPIN STATE POLY(PHENYL)CARBENES

To present a realistic application of our convergence acceleration technique, DMRG-CASSCF calculations were performed on poly(phenyl)carbenes in the lowest singlet and high-spin states. We looked at the three structures shown in Figure 3, $C_{7n+6}H_{4n+6}$, n = 1–3; they will be denoted as n-carbenes (n = 1, 2, or 3), and contain 1, 2, or 3 carbene (-C:-) links. All calculations used the 6-31G basis set. Molecular geometries were optimized by unrestricted-open shell density functional theory of the high-spin state using the B3LYP hybrid exchange-correlation functional. According to our calculations, the ground state is actually the high-spin state, a triplet, quintet, or septet for 1-, 2-, and 3-carbene, respectively. For comparison purposes, we have also made calculations with the BLYP nonhybrid functional, and performed closed shell and restricted open-shell Hartree-Fock (RHF and ROHF) calculations, followed by second-order Mller-Plesset and coupled cluster singles and doubles calculations, without (CCSD) or with (CCSD(T)) perturbative triples corrections. The correlated calculations used the RHF and ROHF reference wavefunctions.

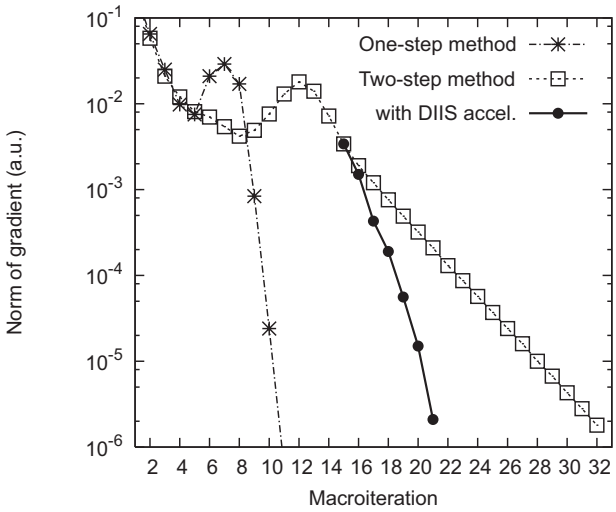

FIGURE 2. Convergence progress of norms of the gradient vectors in CASSCF(10e,10o) calculations for the $^3B_2$ state of SiC_3 with cc-pVQZ basis set.

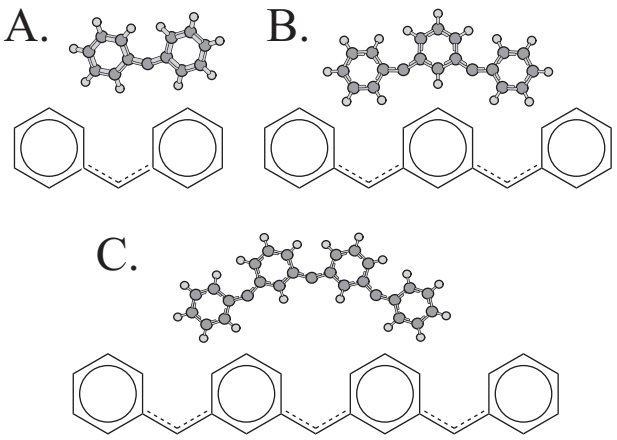

FIGURE 3. Poly(phenyl)carbenes: 1-carbene (a), 2-carbene (b), 3-carbene (c). Molecular structures and geometries optimized with B3LYP/6-31G for the ground states.

For the high-spin state, there are two singly occupied orbitals on each carbene group, as illustrated in Figure 4(a), denoted as sp^2 and p_z orbitals. All unpaired electrons have parallel spins in the high-spin state.

In the singlet state calculations with the RHF and DFT methods, the sp^2 orbitals of each carbene were doubly occupied and the p_z orbitals were empty, as shown in Figure 4(b).

The CAS reference for the DMRG-CASSCF calculations consisted of the valence π orbitals and π electrons on all the carbons. In addition, the sp^2 σ orbitals on each carbene group were included, resulting in CAS calculations of (14e, 14o), (22e, 22o), and (30e, 30o) for the 1-, 2-, and 3-carbenes, respectively. This corresponds to a full active CI dimension of 1.2×10^7, 5.0×10^{11}, and 2.4×10^{16}, respectively.

Table III shows the total energies of *n*-carbene at the high-spin and singlet states along with their energy differences. All the calculations with the single-reference B3LYP, BLYP, HF, MP2, CCSD, and CCSD(T) methods, and the multireference DMRG-CASSCF method predict that the high-spin state energies are lower than the singlet state energies. As to the state energy differences, however, there are significant discrepancies between single-reference and multireference calculations. The energy differences calculated by DMRG-CASSCF were 0.938, 0.302, and 0.728 eV for 1-, 2-, and 3-carbenes, respectively, whereas the high-level single reference calculations with CCSD(T) method yielded surprisingly much larger energy differences such as 1.363, 2.832, and 4.305 eV for the respective carbenes. All the single-reference calculations including DFT described the similar trends of increasingly larger state energy differences for longer carbene chains. Since the state energy differences of the uncorrelated HF method are as large as those of the correlated single-reference MP2, CCSD, and CCSD(T) calculations, the dynamic correlation seems to be irrelevant to the descriptions. Although the DFT calculations predicted slightly smaller energy differences than the other single-reference counterparts, the energy differences obtained by these single-determinant approaches are more or less the same, in contrast to much smaller energy differences of DMRG-CASSCF.

In Table IV, the diagonal elements of the one-particle density matrix in localized basis are shown for sp^2 and p_z orbitals of each carbene of *n*-carbene ($n = 1, 2, 3$) to figure out what gives rise to such a large discrepancy in the state energy differences between the single-reference and DMRG-CASSCF calculations. For the high-spin state, as described earlier, sp^2 and p_z orbitals of each carbene are occupied with the unpaired electrons, which have the parallel spins. This configuration picture of the high-spin state is verified by both single-reference and DMRG-CASSCF calculations, which reproduced the single occupations in the one-electron density matrix elements for the sp^2 and p_z orbitals. Note that the diagonal density matrix elements of p_z orbitals on phenyl groups are found to be nearly 1.

As to the singlet state, the diagonal elements represent clear qualitative differences between the

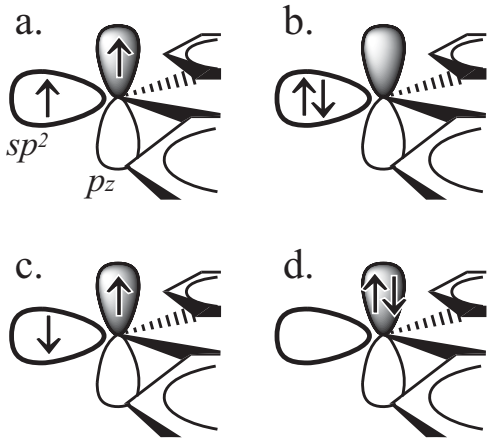

FIGURE 4. sp^2 and p_z orbitals of the carbene in sp^2 hybridization picture and the spin configurations of two valence electrons occupying the orbitals.

TABLE III

Total energies of *n*-carbene (*n* = 1, 2, 3) at the high-spin and singlet states along with the energy differences.

Method	High-spin state energy E_G (hartree)	Singlet state energy E_S (hartree)	Diff. $E_S - E_G$ (hartree)	Diff. $E_S - E_G$ (eV)
1-carbene	Triplet ($S = 1$)	Singlet ($S = 0$)		
B3LYP	−501.190 89	−501.149 04	0.041 85	1.139
BLYP	−500.968 41	−500.928 37	0.040 04	1.090
RHF/ROHF	−497.853 46	−497.803 58	0.049 87	1.357
MP2	−498.949 26	−498.903 33	0.045 93	1.250
CCSD	−499.038 18	−498.985 51	0.052 67	1.433
CCSD(T)	−499.086 73	−499.036 64	0.050 09	1.363
DMRG-CASSCF (14,14)	−498.021 75	−497.987 29	0.034 47	0.938
2-carbene	Quintet ($S = 2$)	Singlet ($S = 0$)		
B3LYP	−770.185 03	−770.097 29	0.087 74	2.388
BLYP	−769.850 77	−769.767 37	0.083 39	2.269
RHF/ROHF	−765.084 99	−764.984 83	0.100 16	2.725
MP2	−766.761 71	−766.664 61	0.097 09	2.642
CCSD	−766.896 36	−766.786 54	0.109 82	2.988
CCSD(T)	−766.971 48	−766.867 41	0.104 07	2.832
DMRG-CASSCF (22, 22)	−765.346 30	−765.335 22	0.011 07	0.301
3-carbene	Septet ($S = 3$)	Singlet ($S = 0$)		
B3LYP	−1039.179 03	−1039.045 37	0.133 66	3.637
BLYP	−1038.733 14	−1038.606 21	0.126 93	3.454
RHF/ROHF	−1032.316 45	−1032.165 81	0.150 64	4.099
MP2	−1034.573 98	−1034.425 70	0.148 28	4.035
CCSD	−1034.754 42	−1034.587 35	0.167 07	4.546
CCSD(T)	−1034.856 16	−1034.697 96	0.158 20	4.305
DMRG-CASSCF (30,30)	−1032.670 74	−1032.656 87	0.013 86	0.377

6-31G basis set is used.

single-reference and DMRG-CASSCF wavefunctions. In the single-determinant RHF description where all electrons have to be paired, sp^2 orbitals are doubly occupied while p_z orbitals of each carbene are unoccupied. Contrarily, the multiconfigurational treatment with the DMRG-CASSCF wavefunction considerably stabilizes the singlet state by capturing multiple important configurations other than the RHF configuration, such as the spin configurations illustrated in Figures 4(b)–(d), which distribute two electrons over sp^2 and p_z orbitals with the similar weights. This reveals that the electronic structure of the singlet state is of very strong multireference character and thus should not be described by the single-reference methods.

It should be repeatedly mentioned that the DMRG-CASSCF numbers do not include dynamical correlation. The quantitative arguments have to be followed by future calculations of dynamical correlation on top of the DMRG-CASSCF multireference wavefunctions, which should be qualitatively correct at the present stage.

4. Conclusion

In this study, we have presented an algorithm that accelerates the convergence of iterative minimization of the two-step CASSCF procedure. The major benefit from the acceleration is to save a number of exact diagonalizations repeated, which are often the dominant computational expense in large-scale CASSCF calculations with the DMRG-CASSCF method, to which the one-step CASSCF optimization is not applicable in practice. The algorithm shown in this work should be easily implemented in the existent two-step CASSCF program codes.

Complex electronic structures are involved in many interesting chemical phenomena in which the

TABLE IV

Diagonal elements of the one-electron density matrix in localized basis for sp^2 and p_z orbitals on each carbene of *n*-carbene (*n* = 1, 2, 3) at the high-spin and singlet states.

	High-spin state		Singlet state	
	ROHF UBLYP UB3LYP	DMRG-CASSCF	RHF RBLYP RB3LYP	DMRG-CASSCF
1-carbene	Triplet ($S = 1$)		Singlet ($S = 0$)	
$1sp^2$	1.	1.000	2.	1.000
$1p_z$	1.	0.983	0.	0.983
2-carbene	Quintet ($S = 2$)		Singlet ($S = 0$)	
$1sp^2$	1.	1.000	2.	1.000
$1p_z$	1.	0.983	0.	0.981
$2sp^2$	1.	1.000	2.	1.000
$2p_z$	1.	0.983	0.	0.981
3-carbene	Septet ($S = 3$)		Singlet ($S = 0$)	
$1sp^2$	1.	1.000	2.	1.000
$1p_z$	1.	0.983	0.	0.981
$2sp^2$	1.	1.000	2.	1.000
$2p_z$	1.	0.983	0.	0.980
$3sp^2$	1.	1.000	2.	1.000
$3p_z$	1.	0.983	0.	0.981

Comparison is made between the single-reference HF/BLYP/B3LYP and multireference DMRG-CASSCF wavefunctions.

multireference natures of strongly interacting electrons must be described by computationally efficient and sophisticated correlation theories. The DMRG-CASSCF with the present acceleration scheme should be one of the most efficient, extensible strong correlation methods that can handle unprecedentedly large degrees of freedom of the complex electron correlations such as CAS(30e, 30o), which would be intractable with other standard methods. The DMRG-CASSCF method should be used primarily to describe the static correlation with optimized orbitals for the large-scale multireference problems. The wavefunction of DMRG-CASSCF can be incorporated as a starting multireference into subsequent dynamical correlation calculations via perturbation theory or canonical transformation theory [63–65] to eventually achieve chemical accuracy for the computational descriptions of the multireference chemical phenomena.

References

1. Yeager, D. L.; Jørgensen, P. J Chem Phys 1979, 71, 755.
2. Jensen, H.-J. A.; Jørgensen, P. J Chem Phys 1984, 80, 1204.
3. Lengsfield, B. H., III. J Chem Phys 1980, 73, 382.
4. Lengsfield, B. H., III. J Chem Phys 1982, 77, 4073.
5. Werner, H.-J.; Meyer, W. J Chem Phys 1980, 73, 2342.
6. Werner, H.; Knowles, P. J Chem Phys 1985, 82, 5053.
7. Werner, H.-J. Adv Chem Phys 1987, 69, 1.
8. Ruedenberg, K.; Schmidt, M.; Gilbert, M.; Elbert, S. Chem Phys 1982, 71, 41.
9. Schmidt, M. W.; Gordon, M. S. Ann Rev Phys Chem 1998, 49, 233.
10. Roos, B. O.; Taylor, P. R.; Siegbahn, P. E. M. Chem Phys 1980, 48, 157.
11. Siegbahn, P. E. M.; Almlöf, J.; Heiberg, A.; Roos, B. O. J Chem Phys 1981, 74, 2384.
12. Roos, B. O. Adv Chem Phys 1987, 69, 399.
13. Shepard, R. Adv Chem Phys 1987, 69, 63.
14. Nakano, H.; Hirao, K. Chem Phys Lett 2000, 317, 90.
15. Hirao, K. Chem Phys Lett 1992, 190, 374.
16. Hirao, K. Chem Phys Lett 1992, 196, 397.
17. Hirao, K. Int J Quantum Chem 1992, S26, 517.
18. Hirao, K. Chem Phys Lett 1993, 201, 59.
19. Nakano, H.; Yamanishi, M.; Hirao, K. Trends Chem Phys 1997, 6, 167.
20. Choe, Y.; Nakao, Y.; Hirao, K. J Chem Phys 2001, 115, 621.
21. Nakano, H. J Chem Phys 1993, 99, 7983.
22. Nakano, H. Chem Phys Lett 1993, 207, 372.
23. Nakano, H.; Nakatani, J.; Hirao, K. J Chem Phys 2001, 114, 1133.
24. Nakano, H.; Uchiyama, R.; Hirao, K. J Comput Chem 2002, 23, 1166.
25. Andersson, K.; Malmqvist, P.; Roos, B.; Sadlej, A.; Wolinski, K. J Phys Chem 1990, 94, 5483.

26. Andersson, K.; Malmqvist, P.; Roos, B. J Chem Phys 1992, 96, 1218.
27. Ghosh, D.; Hachmann, J.; Yanai, T.; Chan, G. K.-L. J Chem Phys 2008, 128, 144117.
28. Zgid, D.; Nooijen, M. J Chem Phys 2008, 128, 144115.
29. Zgid, D.; Nooijen, M. J Chem Phys 2008, 128, 144116.
30. White, S. R. Phys Rev Lett 1992, 69, 2863.
31. White, S. R. Phys Rev B 1993, 48, 10345.
32. White, S. R.; Martin, R. L. J Chem Phys 1999, 110, 4127.
33. Daul, S.; Ciofini, I.; Daul, C.; White, S. R. Int J Quantum Chem 2000, 79, 331.
34. Rissler, J.; Noack, R. M.; White, S. R. Chem Phys 2006, 323, 519.
35. Mitrushenkov, A. O.; Fano, G.; Ortolani, F.; Linguerri, R.; Palmieri, P. J Chem Phys 2001, 115, 6815.
36. Mitrushenkov, A. O.; Linguerri, R.; Palmieri, P.; Fano, G. J Chem Phys 2003, 119, 4148.
37. Chan, G. K. L.; Head-Gordon, M. J Chem Phys 2002, 116, 4462.
38. Chan, G. K. L.; Head-Gordon, M. J Chem Phys 2003, 118, 8551.
39. Chan, G. K. L. J Chem Phys 2004, 120, 3172.
40. Chan, G. K. L.; Kállay, M.; Gauss, J. J Chem Phys 2004, 121, 6110.
41. Chan, G. K. L.; Van Voorhis, T. J Chem Phys 2005, 122, 204101.
42. Hachmann, J.; Cardoen, W.; Chan, G. K. L. J Chem Phys 2006, 125, 144101.
43. Dorando, J. J.; Hachmann, J.; Chan, G. K.-L. J Chem Phys 2007, 127, 084109.
44. Hachmann, J.; Dorando, J. J.; Avilés, M.; Chan, G. K.-L. J Chem Phys 2007, 127, 134309.
45. Chan, G. Phys Chem Chem Phys 2008, 10, 3454.
46. Zgid, D.; Nooijen, M. J Chem Phys 2008, 128, 014107.
47. Moritz, G.; Hess, B. A.; Reiher, M. J Chem Phys 2005, 122, 024107.
48. Moritz, G.; Reiher, M. J Chem Phys 2006, 124, 034103.
49. Moritz, G.; Reiher, M. J Chem Phys 2007, 126, 244109.
50. Nakayama, K.; Nakano, H.; Hirao, K. Int J Quantum Chem 1998, 66, 157.
51. Kawashima, Y.; Nakayama, K.; Nakano, H.; Hirao, K. Chem Phys Lett 1997, 267, 82.
52. Kurashige, Y.; Nakano, H.; Nakao, Y.; Hirao, K. Chem Phys Lett 2004, 400, 425.
53. Pulay, P. Chem Phys Lett 1980, 73, 2.
54. Hamilton, T.; Pulay, P. J Chem Phys 1986, 84, 5728.
55. Alberts, I. L.; Grev, R. S.; Schaefer, H. F., III. J Chem Phys 1990, 93, 5046.
56. Stanton, J. F.; Gauss, J.; Christiansen, O. J Chem Phys 2001, 114, 2993.
57. Rintelman, J. M.; Gordon, M. S. J Chem Phys 2001, 115, 1795.
58. Kurashige, Y.; Nakano, H.; Hirao, K. J Phys Chem A 2004, 108, 3064.
59. Ten-no, S. Chem Phys Lett 2007, 447, 175.
60. Dunning, T. H., Jr. J Chem Phys 1989, 90, 1007.
61. Woon, D. E.; Dunning, T. H., Jr. J Chem Phys 1993, 98, 1358.
62. Werner, H.-J.; Knowles, P. J.; Lindh, R.; Manby, F. R.; Schütz, M.; Celani, P.; Korona, T.; Mitrushenkov, A.; Rauhut, G.; Adler, T. B.; Amos, R. D.; Bernhardsson, A.; Berning, A.; Cooper, D. L.; Deegan, M. J. O.; Dobbyn, A. J.; Eckert, F.; Goll, E.; Hampel, C.; Hetzer, G.; Hrenar, T.; Knizia, G.; Köppl, C.; Liu, Y.; Lloyd, A. W.; Mata, R. A.; May, A. J.; McNicholas, S. J.; Meyer, W.; Mura, M. E.; Nicklass, A.; Palmieri, P.; Pflüger, K.; Pitzer, R.; Reiher, M.; Schumann, U.; Stoll, H.; Stone, A. J.; Tarroni, R.; Thorsteinsson, T.; Wang, M.; Wolf, A. Molpro, version 2006.1, a package of ab initio programs 2006. Available at: http://www.molpro.net.
63. Yanai, T.; Chan, G. J Chem Phys 2006, 124, 194106.
64. Chan, G.; Yanai, T. Adv Chem Phys 2007, 134, 343.
65. Yanai, T.; Chan, G. J Chem Phys 2007, 127, 104107.